Nanojoining — A New Frontier in Welding and Joining of Materials

A review of progress in nanojoining over the past two decades and an exploration of the challenges facing this emerging field

BY Y. N. ZHOU

Abstract

This paper, adapted from the 2024 Comfort A. Adams Lecture presented at the American Welding Society's annual convention on October 14, 2024, in Orlando, Fla., provides an overview of the emerging field of nanojoining, a technology poised to become a cornerstone in manufacturing nano-devices and systems. This review first surveys nanojoining processes developed over the past two decades and then focuses on femtosecond laser nanowelding, covering process physics and materials science issues. Finally, the review suggests future research directions, addressing engineering challenges and fundamental questions in nanojoining.

Keywords

- Nanojoining
- Nanowelding
- Nanobonding
- Nanosoldering
- Nanobrazing

Introduction

Since the founding of the American Welding Society (AWS) by Dr. Comfort A. Adams in 1919, welding technology has made tremendous strides and become an essential part of manufacturing in almost all industries (Ref. 1). However, the welding industry continues to advance, adapting to new challenges and technologies.

One of these challenges is ongoing miniaturization. For example, when the first integrated circuit was invented at Texas Instruments in 1958, its process feature size was around 75 µm. Over 60 years later, this size has been reduced to below 5 nm (Ref. 2). In welding and joining, ultrasonic welding has been one of the major microjoining processes for chip-level interconnections to join Au, Al, or Cu wires of the typical diameter 20 µm. Trillions of wire bonds are currently made each year using this process (Ref. 3). More recently, ultrasonic welding has been explored for joining carbon nanotubes (CNTs) to Ti substrates, paving the way for future nanoelectronics applications (Ref. 4).

Nanojoining not only differs from larger-scale welding and joining in terms of scale but also introduces new principles that enhance our understanding of the science and technology of welding and joining. For example, in laser lap welding, the mechanism of heat generation varies significantly depending on scale. At larger scales, heat originates from the surface of the top workpiece and propagates into the bottom workpiece, joining the two materials (Fig. 1A). In contrast, at the nanoscale, heat generation begins at the gap between two nano-workpieces even though the gap is not directly exposed to the light (Fig. 1B) (Ref. 5). This unique nanoscale mechanism, explained later in this paper, can help avoid potential surface damage, a common issue in larger-scale laser welding.

This paper reviews recent progress in nanojoining and explores the challenges facing this emerging field. First, selected nanojoining processes will be briefly introduced. Then, femtosecond (fs) laser nanowelding will be examined as a case study, focusing on process physics and materials science. Finally, advancements in the science and technology of nanojoining will be summarized, and opportunities for future research and development will be identified.

Nanojoining Processes

The purpose of welding and joining is to create a permanent connection between workpieces by forming primary (occasionally secondary) chemical bonds at the faying surfaces

https://doi.org/10.29391/2025.104.022

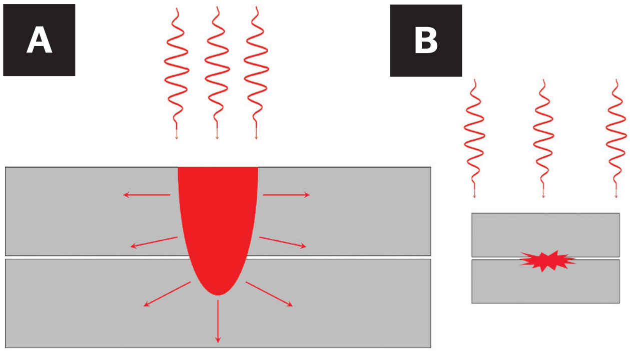

Fig. 1 — Schematic illustrating the differences in laser heating at: A — The micro- and macroscale; B — the nanoscale.

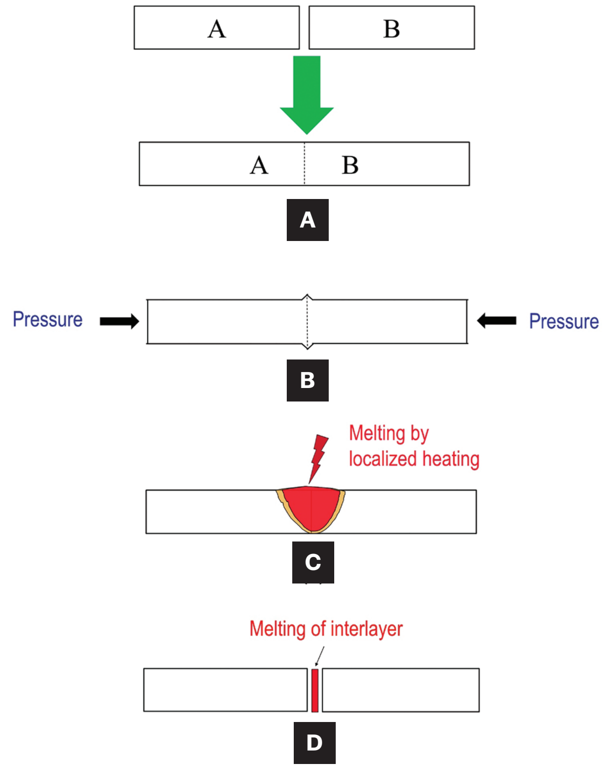

Fig. 2 — Schematic showing: A — Two workpieces before and after welding, and various welding and joining processes including: B — solid state bonding; C — fusion welding; D — brazing and soldering.

(Ref. 1).This principle remains unchanged even when workpieces (i.e., building blocks) are reduced to the nanoscale and microscale (Refs. 6, 7).

Taking a simple butt joint as an example, welding and joining is to replace two faying surfaces with a newly formed interface (Fig. 2A). This process is thermodynamically feasible if the free energy of the interface is lower than the sum of the two original surfaces. A clear example of this principle is wafer bonding, where two perfectly clean and flat Si surfaces with the same atomic orientations can bond at room temperature without external forces (Ref. 8). However, for most engineering materials, heat and/or pressure is needed to remove surface oxides and other contaminants to overcome the influence of surface roughness and lattice mismatching (Refs. 1, 6).

As welding and joining fundamentally involve interfaces, the significance of interfacial regions increases as the workpieces shrink to the nanoscale, making the role of interfaces even more crucial in nanojoining. The phrase "Interface is the device!" appropriately describes how interfacial properties influence nanodevice performance, as will be discussed later.

There are three major welding and joining processes: solid-state bonding, soldering/brazing, and fusion welding (Refs. 1, 6), as shown in Figs. 2B–D. Solid-state bonding is mainly achieved by applying pressure, with heat used to assist in joint formation but remaining below the melting points of the workpieces; in fusion welding, localized melting of workpieces takes place, whereas in brazing/soldering, only the interlayer melts. The distinction between brazing and soldering lies in temperature: brazing occurs above 450°C, whereas soldering is conducted below this threshold (Ref. 1).

Most nanojoining processes (Table 1) developed in the past two decades can still be categorized into these traditional groups (Ref. 7). However, some exceptions exist, such as electron beam nanowelding of CNTs, which will be discussed later (Ref. 9). The following section briefly introduces selected nanojoining processes from Table 1.

Solid State Bonding

Cold pressure nanowelding was employed to join Au nanowires inside a TEM (transmission electron microscopy) vacuum chamber with an STM (scanning tunneling microscopy) probe to add force, as shown in Fig. 3 (Ref. 10). The end-to-end joint strength reached 580 MPa, nearly matching the base nanowire's 600 MPa and much higher than the 100 MPa strength of bulk gold. Cold nanowelding was observed to occur more easily when the two nanowires shared the same lattice orientation at the faying surfaces (Ref. 10). In contrast, cold welding of Ag nanowires required much higher force (pressure) because of the existence of surface oxides, which was applied by a nano-indenter and resulted in large wire deformation, as shown in Fig. 4 (Ref. 11).

Chemical nanowelding has been developed to join various metallic nanowires (Ag, Cu, Ni, Fe or Co) at room temperature without the application of pressure. For example, chemical vapors such as hydrogen peroxide, which condense preferentially at the faying surfaces, can remove surface contaminants (mainly oxides) to enable cold welding (Ref. 13). However, like many other welding and joining processes, excessive etching can lead to over-welding, which should be avoided, as shown in Fig. 5 (Ref. 13).

Ultrasonic nanowelding was applied to join CNTs to Ti electrodes to develop carbon high-efficiency CNT-based photovoltaic cells, shown in Fig. 6 (Ref. 4). The process resulted in a low Ohmic contact between the Ti electrodes and CNTs due to the formation of covalent Ti–C bonds, similar to the reaction layer formed in reactive brazing between ceramics and metals (Ref. 4). This effect is further demonstrated by the significant reduction in resistance across the electrodes

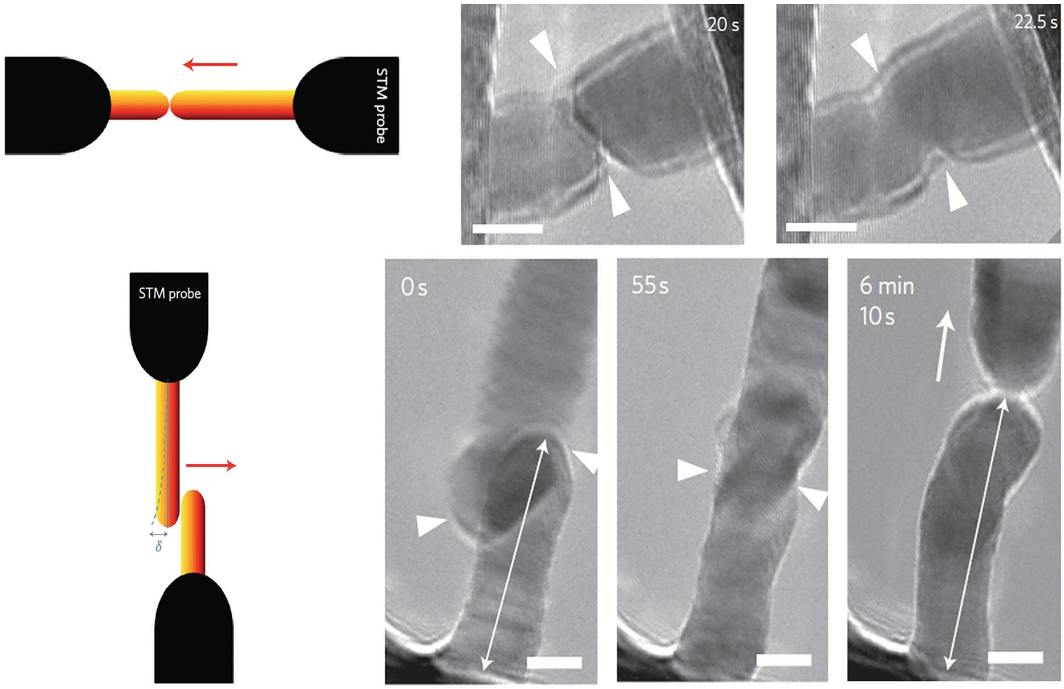

Fig. 3 — Cold welding of AU nanowires: schematic configurations and SEM images (scale bars, 5 nm) of the end-to-end (top row) and side-to-side (bottom row) configurations (Ref. 10).

and the x-ray photoelectron spectroscopy (XPS) spectra in Fig. 6, where the resistance dropped considerably when the ultrasonic power was sufficient to form Ti–C compounds.

Electron beam nanowelding has been developed to join CNTs. In this work (Ref. 9), a focused electron beam was directed to induce structural defects (vacancies and interstitials) at the crossing point of two CNTs. During subsequent heat treatment at 800°C, self-rearrangement of the affected carbon atoms led to the formation of heptagonal or octagonal rings, resulting in inter-nanotube junctions (Fig. 7). The driving force behind this junction formation is the system's energy reduction, as confirmed by molecular dynamics simulations (Ref. 9). While debatable, one could argue that this direct CNT joining process qualifies as solid-state bonding, given that no melting occurs (Table 1).

Resistance nanowelding has been successfully utilized to join graphene sheets in an edge-to-edge configuration by joule heating (Ref. 14). Similar to electron beam nanowelding of CNTs, resistance heating generated dangling bonds at the graphene edges, enabling interconnection and forming a strong, conductive joint between two graphene sheets. However, attempts to join graphene sheets in a layer-to-layer configuration were unsuccessful, as Joule heating could not overcome the energy barriers required to generate dangling bonds. It would be interesting to explore whether an electron beam could be used to create these dangling bonds, a necessary precondition for joining, as demonstrated in the case of electron beam nanowelding (Ref. 9).

Joining with nanomaterials is a solid-state nanojoining process in which nanomaterials, such as nanoparticles, are sintered to form networks while simultaneously bonding to substrates, all driven by diffusion to reduce surface area. In theory, the bonding temperature can be lowered to room temperature due to enhanced diffusion at the nanoscale, significantly reducing bonding temperatures, an important factor for low-temperature bonding in polymer-based microelectronics applications.

However, surface coatings, typically polymer-based (e.g., polyvinylpyrrolidone, PVP), are commonly applied to prevent nanoparticle self-coalescence during long-term storage and handling at room temperature. As a result, elevated temperatures (e.g., 300°C in Cu-to-Cu bonding with Ag nanoparticles [Ref. 15]) are required to decompose these coatings before or during bonding. To address this challenge, a water-based paste of Ag nanowires with a significantly reduced PVP coating has been successfully used to join Cu wire to Cu substrates at room temperature (Ref. 16). It was suggested that this carefully controlled PVP coating could act as a reducing agent, cleaning the Cu surface oxide and promoting Ag-Cu bonding. Additionally, the energy contributions from various nanoscale reactions—including Cu-Ag reaction, Cu oxidation, and CuO deoxidation—could lead to localized heating, enabling bonding while maintaining a globally low temperature (Ref. 16).

Soldering and Brazing

Various nanosoldering and nanobrazing processes have been developed to join nanomaterials and nanoscale building blocks by different heating sources, including reflow oven nanosoldering (Ref. 17), resistance nanosoldering (Refs. 18,

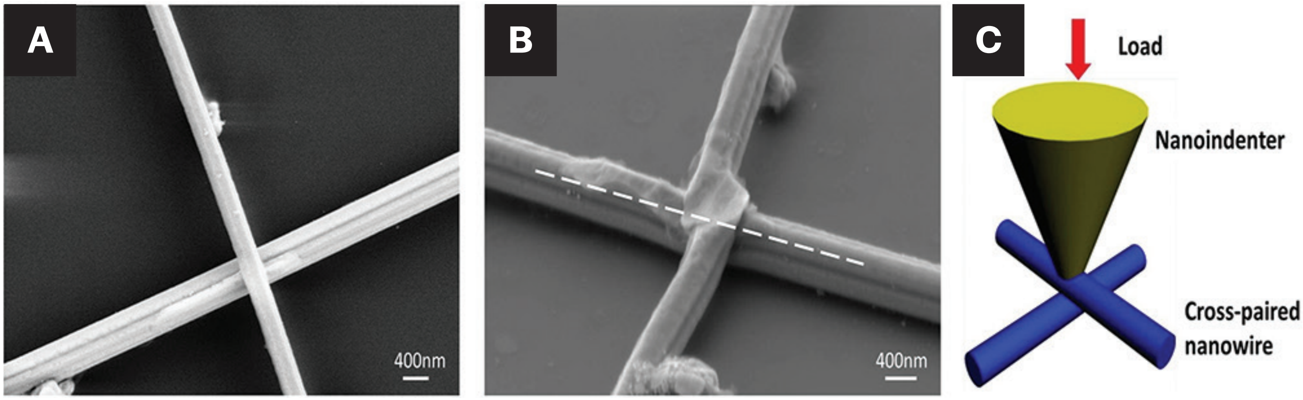

Fig. 4 — Cold welding of Ag nanowires: A — Before welding; B — after welding; C —schematics showing the welding setup with a nano-indenter applying force (Ref. 11).

Table 1 — Nanojoining Processes	
Solid State Bonding	Cold pressure nanowelding Au nanowires (Ref. 10), Ag nanowires (Ref. 11)
	Self-oriented bonding of Ag nanowires (Ref. 12)
	Chemical nanowelding of metallic nanowires (Ref. 13)
	Ultrasonic nanowelding of CNT to Ti (Ref. 4)
	Electron beam nanowelding of CNTs (Ref. 9)
	Resistance nanowelding of graphene (Ref. 14)
	Joining by sintering Ag nanoparticles (Ref. 15) and nanowires (Ref. 16)
Brazing/Soldering	Reflow soldering of Sn-coated Au-Ni-Au nanowires (Ref. 17)
	Resistance soldering of TiO_2 nanowires using $Au_{80}Sn_{20}$ solder (Ref. 18), Pt-Co nanowires with $Sn_{95}Au_5$ solder (Ref. 19)
	Laser brazing of Pt nanoparticles with Au (Ref. 20) and Ag (Ref. 21) nanoparticles
Fusion Welding	Resistance welding of Pt nanowires (Ref. 22), Pt nanowires to Au wires (Ref. 23)
	Laser welding of Au nanoparticles (Ref. 24), Ag nanowires (Ref. 25), Al/Ni nanoparticles (Ref. 26), Ag/Fe nanoparticles (Ref. 27), Au/TiO_2 nanowires (Ref. 5), ZnO nanowires (Ref. 28), ZnO/CuO nanowires (Ref. 29)
	Nano-thermite joining (Ref. 30)

19) and laser nanobrazing (Ref. 20). For example, molten $Au_{20}Sn_{80}$ solder, generated by resistance heating, was successfully applied to join TiO_2 nanowires but was ineffective for SiO_2 nanowires because of the poor wetting behavior, as shown in Fig. 8 (Ref. 18).

These processes, which typically involve forming a single joint at a time, can be slow and costly because of the requirements for accurate manipulation of components and controlled joining operations. As an alternative, batch processes such as reflow soldering allow multiple joints to be formed simultaneously, improving efficiency. For example, Sn/Au/Ni-coated Au nanowires were successfully reflow-soldered together in a liquid medium (Ref. 17).

In another study, a pulsed nanosecond laser was used to melt Au nanoparticles, which then brazed together Pt nanoparticles to form three-dimensional networks, shown in Fig. 9 (Ref. 20). The fact of the optical absorption spectrum of Au and Pt nanoparticles before laser irradiation exhibiting a characteristic peak of the surface plasmon band at 520 nm (Fig. 9A) will be discussed later. Additionally, a femtosecond laser was employed to braze Pt nanoparticles by molten Ag (Ref. 21).

Crossing multiwalled CNTs were joined by irradiating the junction inside a SEM, as shown in Fig. 10 (Ref. 31). This pro-

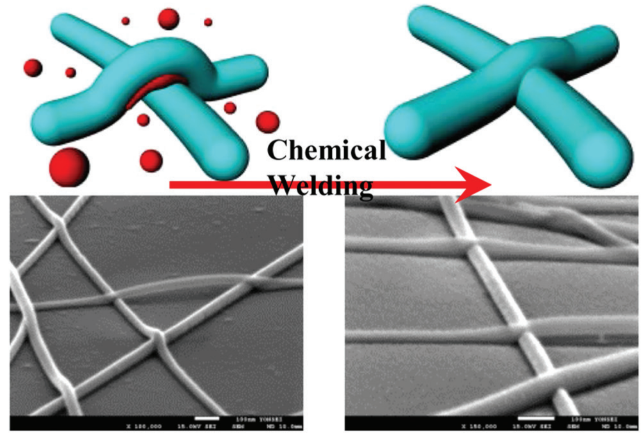

Fig. 5 — Schematic showing the preferential condensation of chemical vapors, such as hydrogen peroxide, at the faying surfaces, promoting cross-wire welding. SEM images show nanowires before and after welding (Ref. 13).

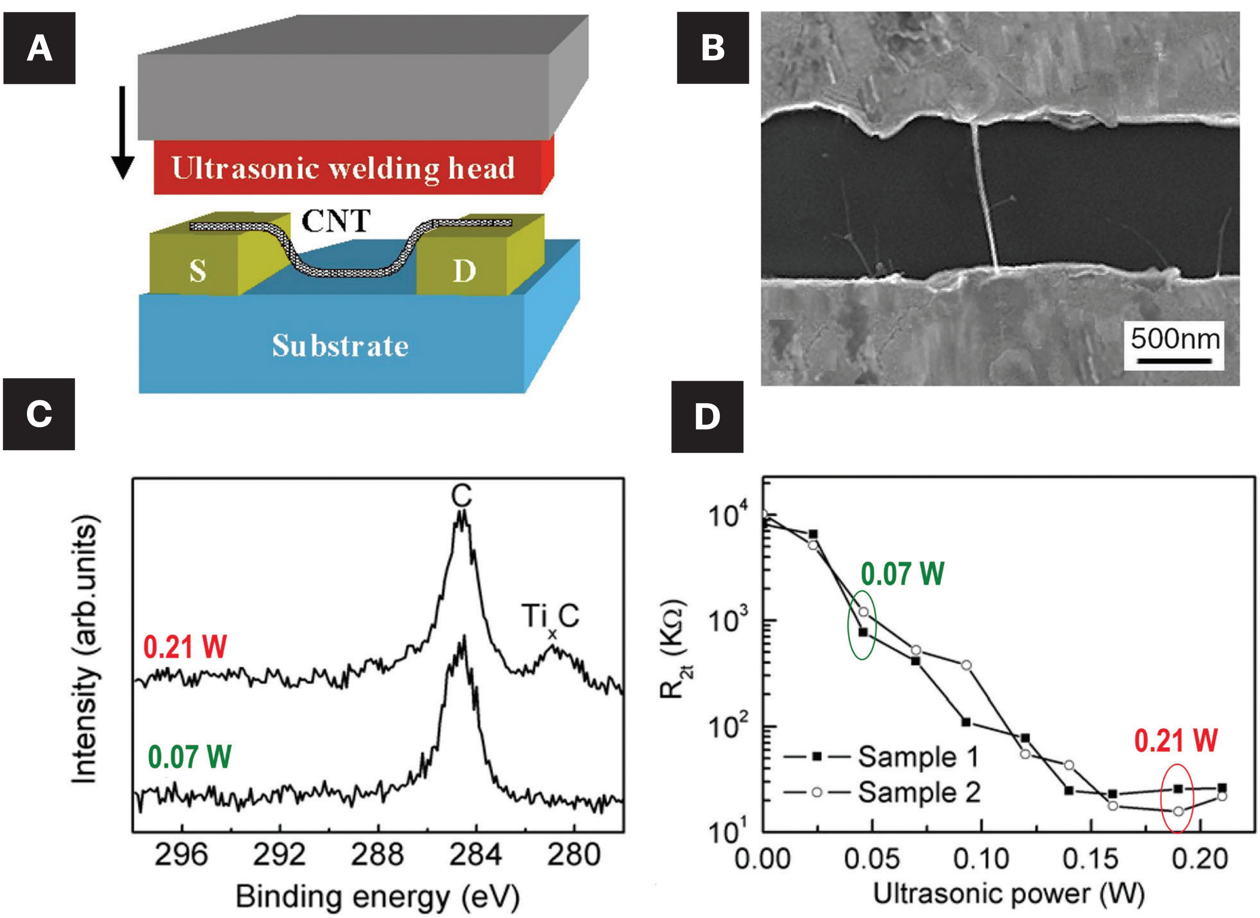

Fig. 6 — A — Schematic of the ultrasonic nanowelding setup, showing a clamping force (indicated by the arrow) pressing the welding head against the nanotube, along with Ti electrodes (S and D); B — SEM images of CNTs welded onto the Ti electrodes; C — XPS spectra of the weld zone at ultrasonic powers of 0.07 W and 0.21 W; D — two-terminal resistance across the electrodes as a function of ultrasonic power (Ref. 4).

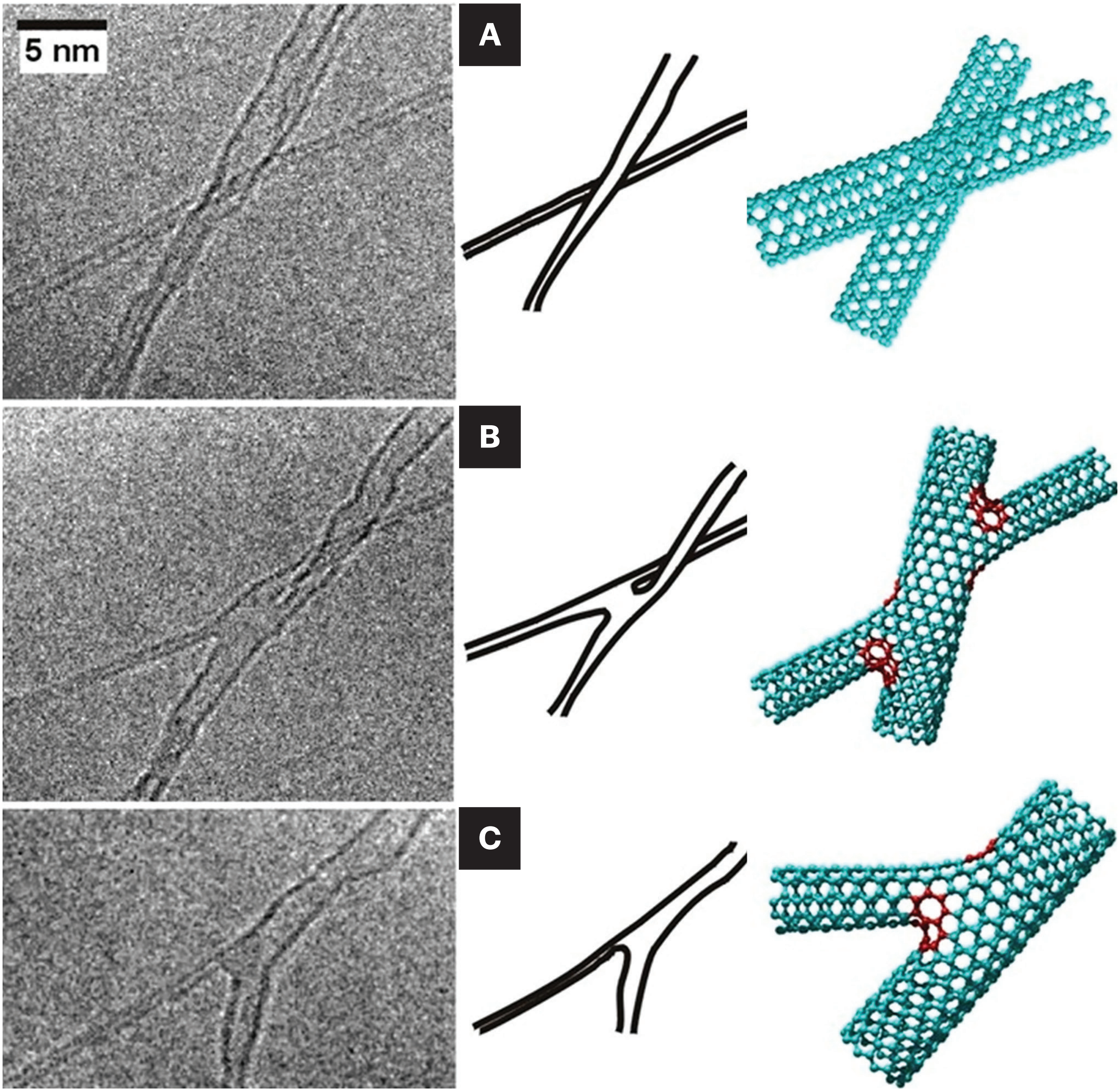

Fig. 7 — A — A single-wall CNT crossing another single-wall CNT; B — after 60 s of electron irradiation and subsequent heat treatment, connections form between the two tubes, creating "X" and "Y" junctions. Schematics illustrating molecular models are provided for each image. Heptagonal rings are highlighted in red (Ref. 9).

cess involved the aggregation of hydrocarbons, followed by their transformation into amorphous carbon under the electron beam. Although this technique was termed as "soldering" (Ref. 31), it seems to more closely resemble adhesive bonding (Ref. 1).

Fusion Welding

Fusion nanowelding processes have been developed using various heat sources, including resistance heating (Refs. 22, 23), laser beam (Refs. 24-29), and even nanothermite (Ref. 30). As shown in Fig. 11, two Pt nanowires were welded through the resolidification (fusion) of the molten metal at the faying surfaces produced by Joule heating (Ref. 22). This resistance nanowelding method has also been used to join dissimilar metals, such as welding Pt nanowire to a thin Au wire to create heterojunctions (Ref. 23). Detailed discussions on ultrafast laser nanowelding are in the next section.

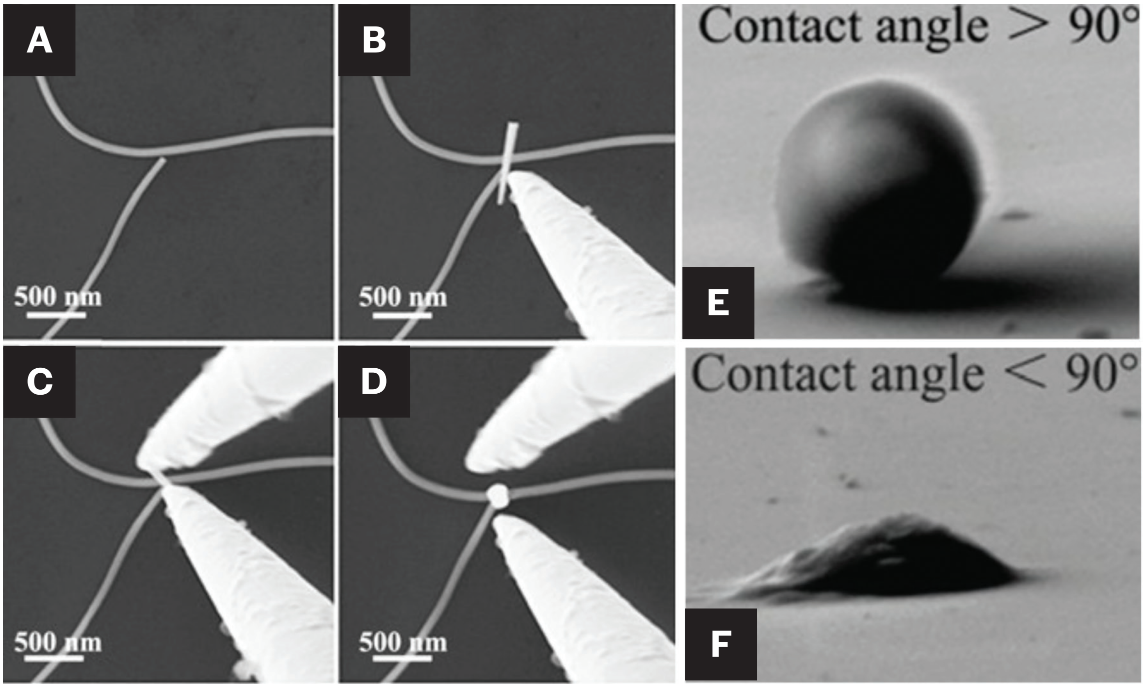

Fig. 8 — SEM images of: A — TiO_2 nanowire assembly before soldering; B — placement of $Au_{80}Sn_{20}$ nanosolder by nanomanipulators; C — resistance soldering of the nanowires; D — soldered nanowires; and the lateral profile of a melted nanosolder on: E — SiO_2 and F — TiO_2 substrates (Ref. 18).

Ultrafast Laser Nanowelding (A Case Study)

Nanowelding with lasers of ultrashort laser pulses (shorter than picoseconds), also known as ultrafast lasers, is reviewed here as a separate case study for two reasons. First, laser nanowelding is one of the most widely used nanojoining processes. Second, the interaction between ultrafast laser and materials is fundamentally different, governed by non-thermal phenomena (Ref. 32).

Heat Generation at "Hot Spots"

The focal diameters of typical laser beams used for welding range from tens to hundreds of micrometers (µm), which is significantly larger than nanoscale building blocks (Fig. 12). This might suggest that localized melting, confined to the gap region, would be impossible. However, nature provides a different mechanism, localized surface plasmon resonance (LSPR), which enables the focusing of laser light at the gaps between nanocomponents (Ref. 25).

When incident light interacts with metallic nanocomponents, it induces internal electron polarization and oscillation within the material. LSPR occurs when the frequency of the collective oscillation of conduction electrons (plasmons) matches that of the incident light, leading to constructive interference. This effect enhances the electric field in localized areas, particularly at high-curvature surfaces and junctions/gaps between nanocomponents, creating "hot spots." These hot spots can amplify the local electric field by up to 10^4 times, significantly increasing the absorption and scattering of light. As a result, LSPR provides a foundation for nanoscale manipulation of light, heat, and force. This is why laser joining of metallic nanocomponents based on LSPR is also called plasmonic nanowelding. Referring back to Fig. 9A, a laser of 532 nm is perfect for melting Au nanoparticles since it is close to the surface plasmon band of Au nanoparticle at 520 nm.

A compelling example of how LSPR facilitates nanojoining is a study on the joining of Ag nanowires, where a tungsten halogen lamp, rather than a focused light source, was used to illuminate crossed Ag nanowires (Ref. 25). In this process, the gaps (hot spots) between the nanowires preferentially absorbed photons, generating localized heat that induced fusion welds at the junctions (Fig. 13). In essence, these hot spots acted as nanoscale antennas, concentrating light precisely where the joints needed to form.

Non-Thermal Phenomena

Ultrafast introduces two key effects: increased power density and non-thermal phenomena. The power density of a femtosecond (fs) laser can be up to 10^6 times higher than that of a nanosecond (ns) laser, resulting in significantly reduced heat loss and minimal damage to nanocomponents (Ref. 33).

Non-thermal effects occur when the laser pulse duration is shorter than a few picoseconds (ps), the time required for energy transfer from electrons to the lattice. Under these conditions, material transformations such as melting and phase transitions take place without significant heating of the lattice, as illustrated in Fig. 14 (Ref. 34). In contrast, lasers with pulse durations much longer than a few picoseconds

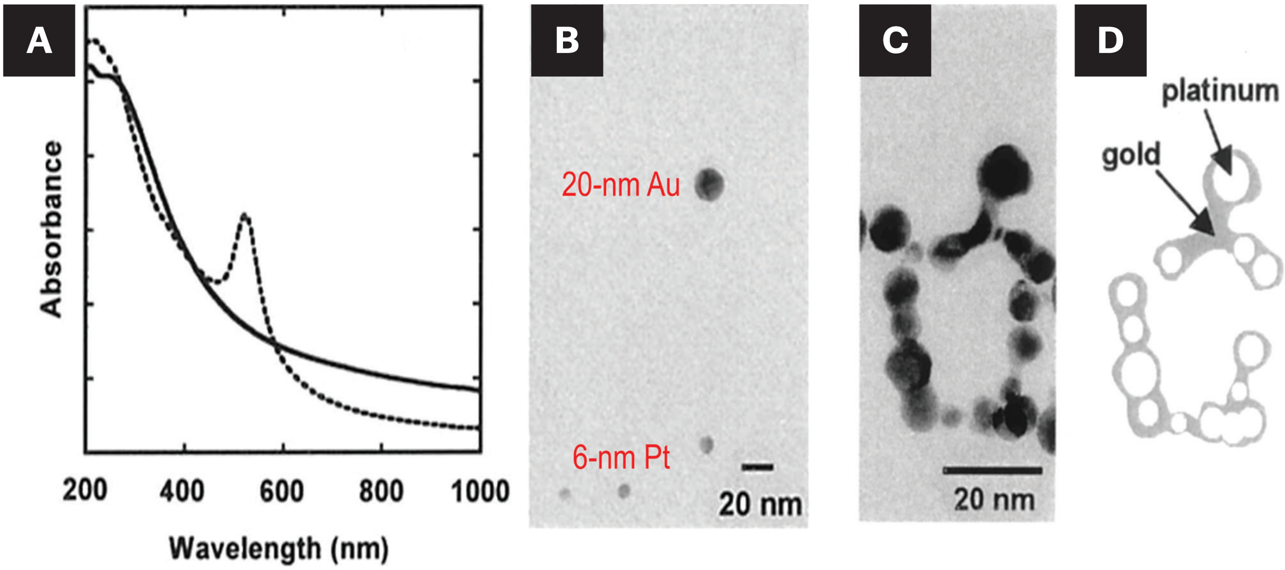

Fig. 9 — A — Optical absorption spectra of mixed 20-nm-Au and 6-nm-Pt nanoparticles produced before (dotted line) and after (solid line) irradiation of a 532-nm laser. Electron micrographs of Au and Pt nanoparticles: B — before; C — after laser irradiation; D — schematic of brazed nanostructures (Ref. 20).

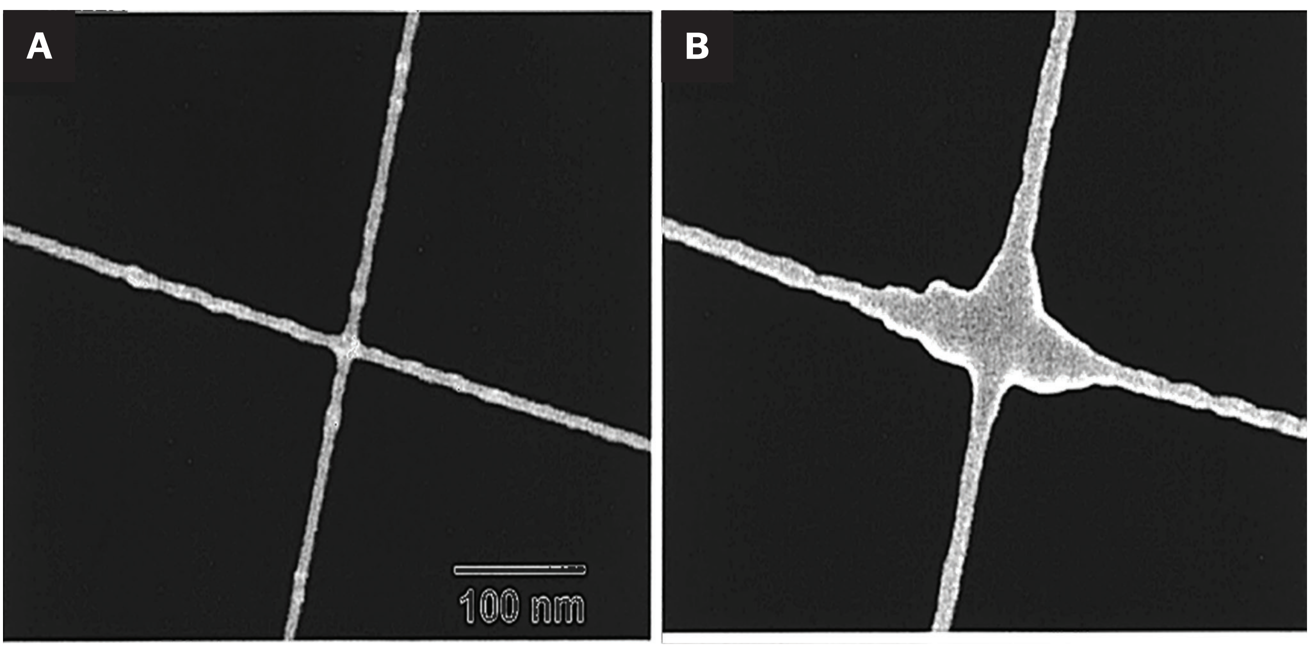

Fig. 10 — SEM images of a nanotube junction: A — Before; B — after "soldering" by deposition of amorphous carbon (Ref. 31).

induce thermal phenomena, where melting occurs due to heat transfer through the lattice.

It has been suggested that molten materials formed via non-thermal mechanisms exhibit properties distinct from those of conventionally melted materials (Ref. 32). However, there is currently no experimental evidence confirming these differences. More importantly, it remains unclear how non-thermal phenomena influence the joining process and the properties of the resulting joints. Further research is needed to explore these effects.

Process Parameters

Similar to laser joining at larger scales, laser nanojoining involves various process parameters, including laser wavelength, pulse duration, intensity, and weld time. However, two factors are particularly critical in laser nanojoining: the gap between nanocomponents and light polarization.

The gap between nanocomponents is one of the key LSPR "hot spots," where photons interact intensely with the materials, significantly influencing heat generation. As

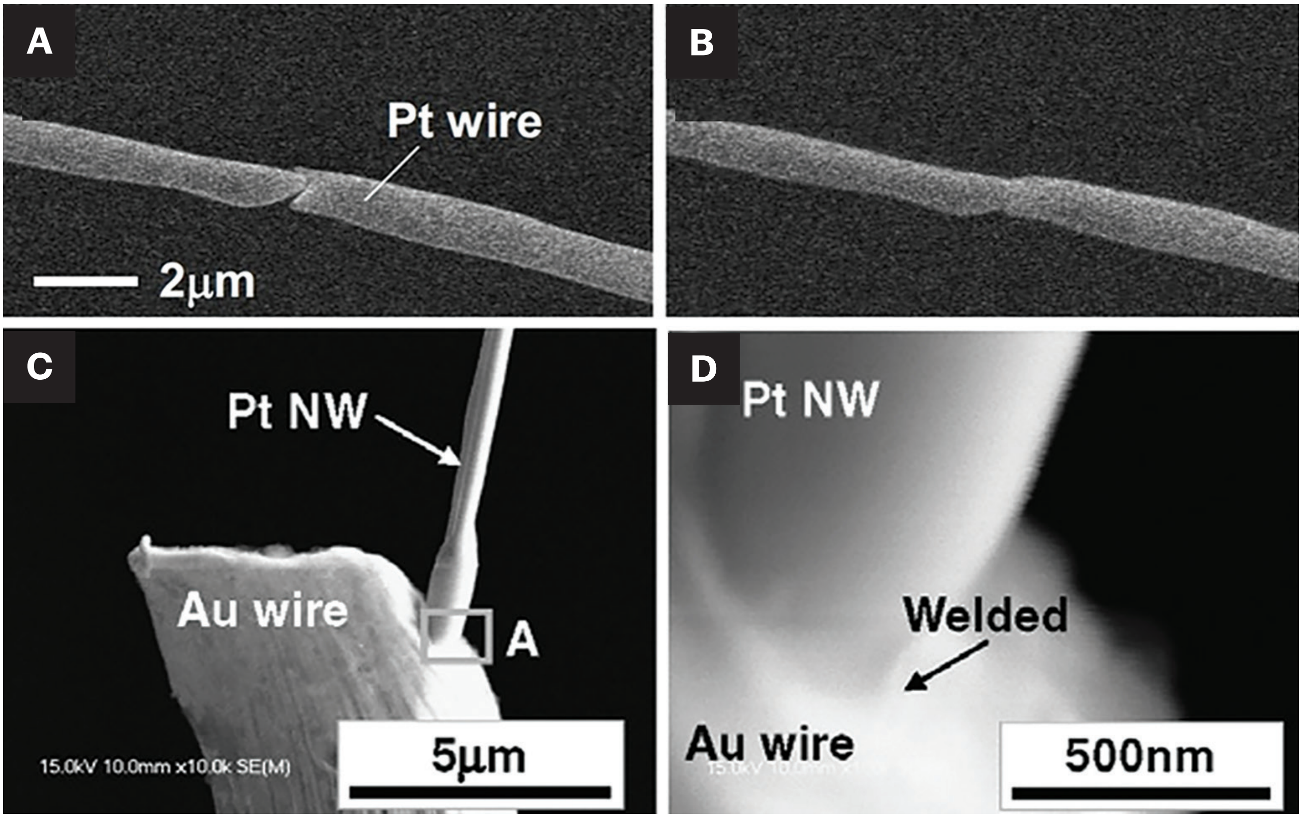

Fig. 11 — SEM images of resistance welding of Pt nanowires (Ref. 22): A — Before welding; B — after welding. Additional SEM images show: C — a Pt nanowire welded to an Au wire; D — a magnified view of region A in C (Ref. 23).

shown in Fig. 15, simulations indicate that heat generation increases as the gap between Ag nanowires decreases, reaching a maximum at approximately 2 nm. Beyond this point, heat generation decreases as further gap reduction leads to melting and collapse of the wires, effectively creating a self-limiting process (Ref. 25).

Heat generation is also highly sensitive to the polarization direction, with higher heat generation occurring when the polarization is perpendicular to the top wire, as shown in Fig. 15 (Ref. 25). This phenomenon helps explain the process window defined by the gap and the angle between two Ag nanowires. As the angle increases and the gap decreases, the process window expands, as illustrated in Fig. 16 (Ref. 35).

Materials Issues

Both miscible Al/Fe nanoparticles and immiscible Ag/Ni nanoparticles have been successfully joined by fs laser processing (Refs. 26, 27). In the case of Al and Fe, bonding occurred through the intermixing of the two elements at the interface. At the same time, the remaining nanoparticles were untouched by the laser (Fig. 17). The formation of amorphous layers at the Al/Fe interface resulted from both intermixing and fast cooling. However, it remains an open question whether this amorphous phase is truly "non-thermal" and how it differs from thermally formed amorphous structures.

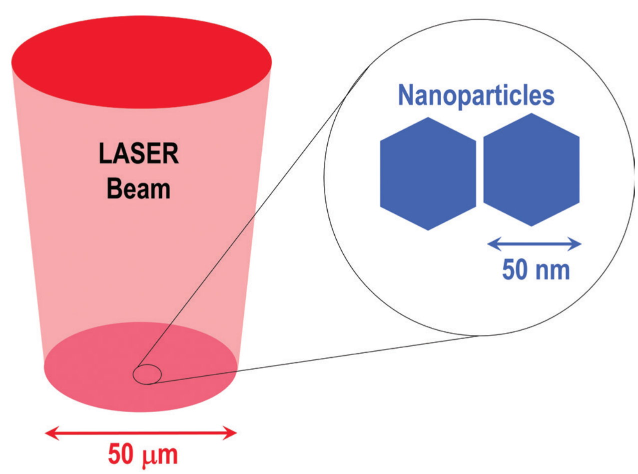

Fig. 12 — Schematic showing that no laser beam can be focused down to the nanometer scale to match the size of nanogaps.

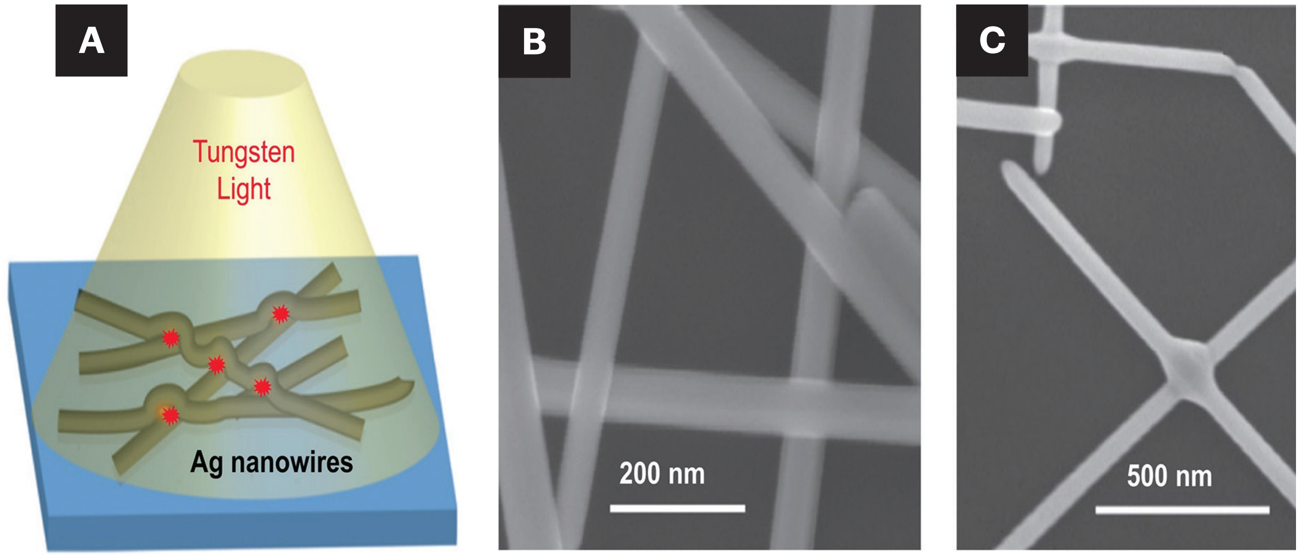

Fig. 13 — A — Schematic illustrating small gaps between crossed Ag nanowires acting as "hot spots" that enable localized heating (red spots). SEM micrographs of Ag nanowires: B — before; C — after welding (Ref. 25).

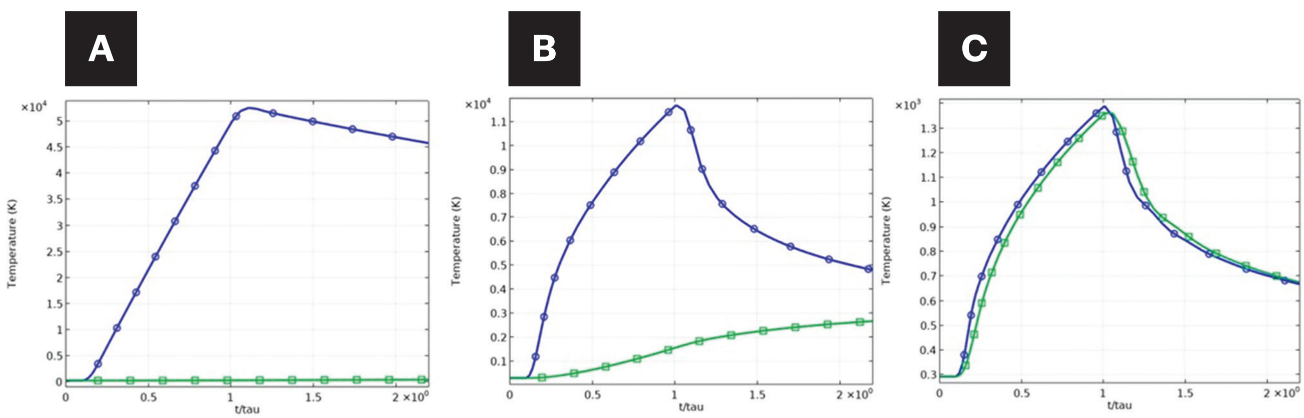

Fig. 14 — Electron (blue) and lattice (green) temperature evolution during laser impact of stainless steel at different pulse durations: A — 100 fs; B — 10 ps; C — 1 ns (Ref. 34).

For immiscible Ag/Ni nanoparticles, direct bonding was observed at the interface, where lattice offsets and structural ledges formed to accommodate atomic misfit (Fig. 18). This supports the argument that interfacial free energy reduction, rather than mutual solubility (mixing or diffusion), is a key criterion for adhesion and bonding (Ref. 36). However, an important question remains: How does ultrafast laser joining of Ag and Ni differ from thermal processing using a longer pulse laser, such as a nanosecond laser? Further research is needed to explore these differences.

While plasmons are considered the primary mechanism for heat generation in laser joining of metallic nanocomponents, and possibly even in metal-to-nonmetal nanocomponent joining, excitons are believed to play a key role in heat generation for non-metallic nanocomponents (Ref. 28).

An exciton is a bound state of an electron and an electron hole, attracted to each other by the electrostatic Coulomb force. It is an electrically neutral quasiparticle that exists in insulators and semiconductors. As shown in Fig. 19, ZnO nanowires before and after femtosecond laser irradiation suggest that the joint was formed through surface melting. However, excessive energy density led to overwelding (cracking) of the nanowires (Ref. 37).

Applications

Nanowelding using ultrafast lasers holds great potential for various applications. One example is the laser assembly of Ag nanoparticle structures, which enhances Raman scattering signals in the surface-enhanced Raman scattering technique (Ref. 38). Another promising application is laser-welded TiO_2/Au nanostructures for memristor-based technologies, including random access memory (ReRAM) and artificial intelligence computing (Ref. 5).

A memristor, or memory resistor, is an emerging nano-device first predicted in 1971 (Ref. 39) and later experimentally

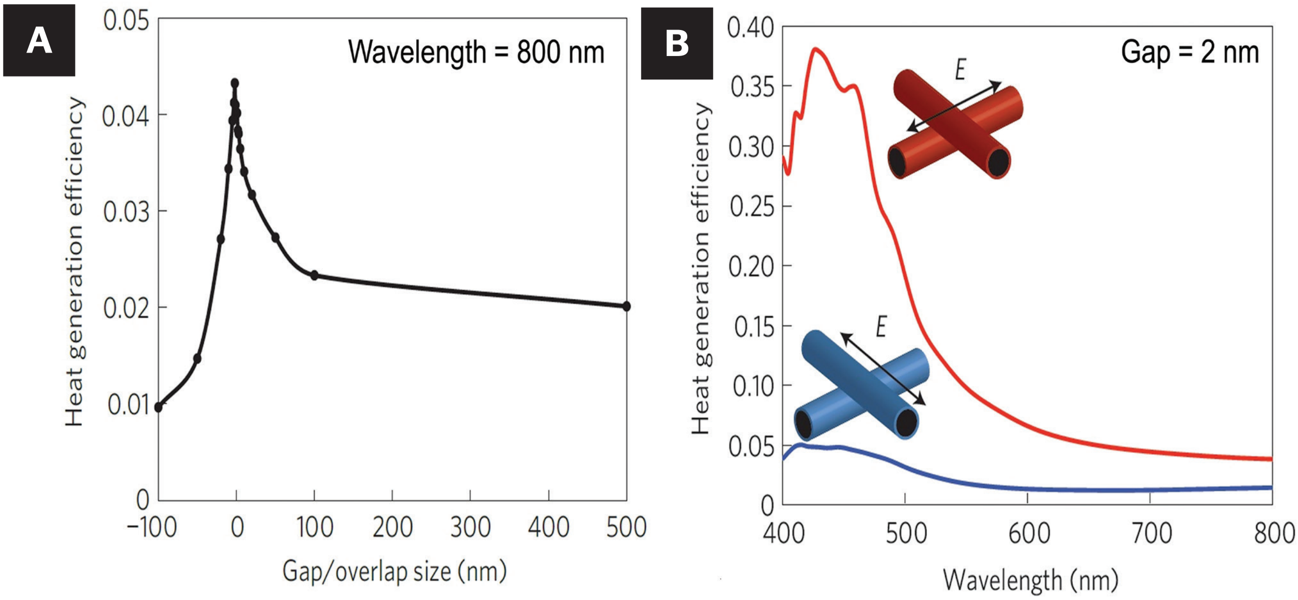

Fig. 15 — Finite element simulations of heat generation at Ag nanowire junctions during plasmonic nanowelding: A — Total heat generation efficiency as a function of gap/overlap size. Negative values on the x axis correspond to interpenetrating nanowires after melting; B — heat generation efficiency as a function of wavelength for light polarized perpendicular (red) or parallel (blue) to the top nanowire in a junction with a 2-nm gap (Ref. 25).

demonstrated in 2008 (Ref. 40). This technology has attracted significant interest for its potential applications in neuromorphic computing and next-generation memory storage.

Figure 20 illustrates an fs-laser-welded TiO_2 nanowire on Au electrodes, forming a memristor and highlighting the heat generation during welding (Ref. 5). Localized plasmonic heating not only facilitated metallurgical heterojunction formation between TiO_2 and Au but also produced functional TiO_{2-x} interfacial layers, as shown in Fig. 21A. This carefully engineered Au/TiO_{2-x}/TiO_2/TiO_{2-x}/Au structure is crucial for achieving the hysteresis I-V characteristics required for memristor behavior (Ref. 5).

However, excessive laser energy led to over-welding, which altered the I-V characteristics, preventing the current hysteresis effect essential for memristor function (Fig. 21B). This study exemplified the critical role of interfacial structures in determining the performance of assembled nanodevices, perfectly capturing the phrase, "Interface is the device!" This example also illustrated that nanojoining is more concerned with electrical and magnetic characteristics while mechanical properties are often the focuses of larger-scale welding and joining (Ref. 1).

Moreover, plasmonic nanowelding is highly advantageous for simultaneously creating connections in large-scale crossbar structures (Fig. 22). Such memristor-based architectures have been proposed for in-memory computing applications (Ref. 41).

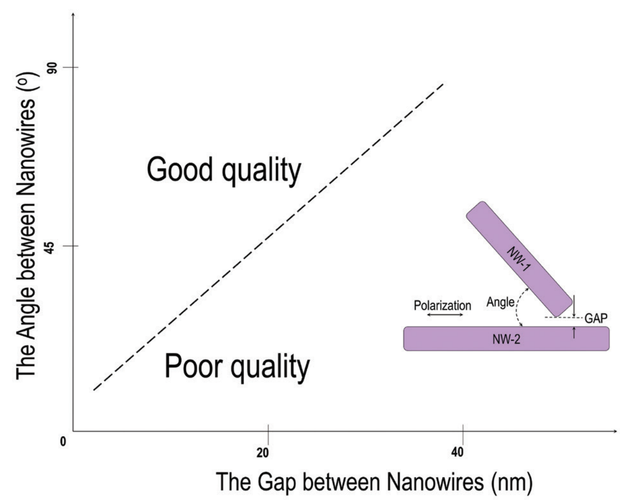

Fig. 16 — Schematic of process window for laser end-to-side joining of Ag nanowires.

Summary and Outlook

Nanojoining is an emerging field poised to become a cornerstone of nano-device and system manufacturing. By evolving beyond traditional welding and joining paradigms, nanojoining emphasizes the critical role of interfaces, captured in the phrase, "Interface is the device!" Compared to large-scale welding, interface properties play an even more crucial role in determining the performance and functionality of nanodevices. Nanojoining presents both familiar and unique challenges compared to conventional welding and joining techniques:

- Precision manipulation: Ensuring accurate alignment and spatial control of nanoscale building blocks.
- Energy source management: Delivering precise energy and heat tailored to nanoscale geometries and material properties.

■ Process sensing and control: Integrating advanced sensing technologies, such as ultra-sensitive temperature probes, for real-time monitoring.
■ Functionality and reliability: Addressing fundamental research gaps to ensure robust and reliable nanostructures. While mechanical properties are often the focuses of larger-scale welding and joining, nanojoining is more concerned with electrical and magnetic characteristics.

Nanojoining also raises fundamental scientific questions, using femtosecond (fs) laser nanowelding as an example:
■ Laser-material interactions: How do metals and non-metals respond differently to laser excitation? What roles

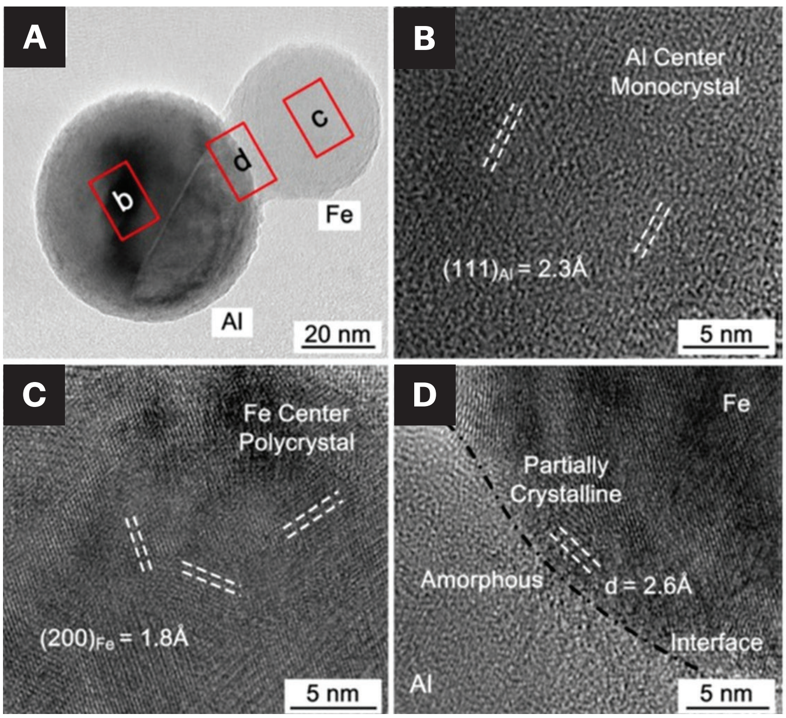

Fig. 17 — High-resolution TEM images of Al-Fe nanoparticles joined by fs laser radiation. A — Morphology of joined Al-Fe nanoparticles with letters indicating corresponding high-resolution images of the red-squared regions b–d; E — schematic of the joint, highlighting the amorphous interfacial region (Ref. 26).

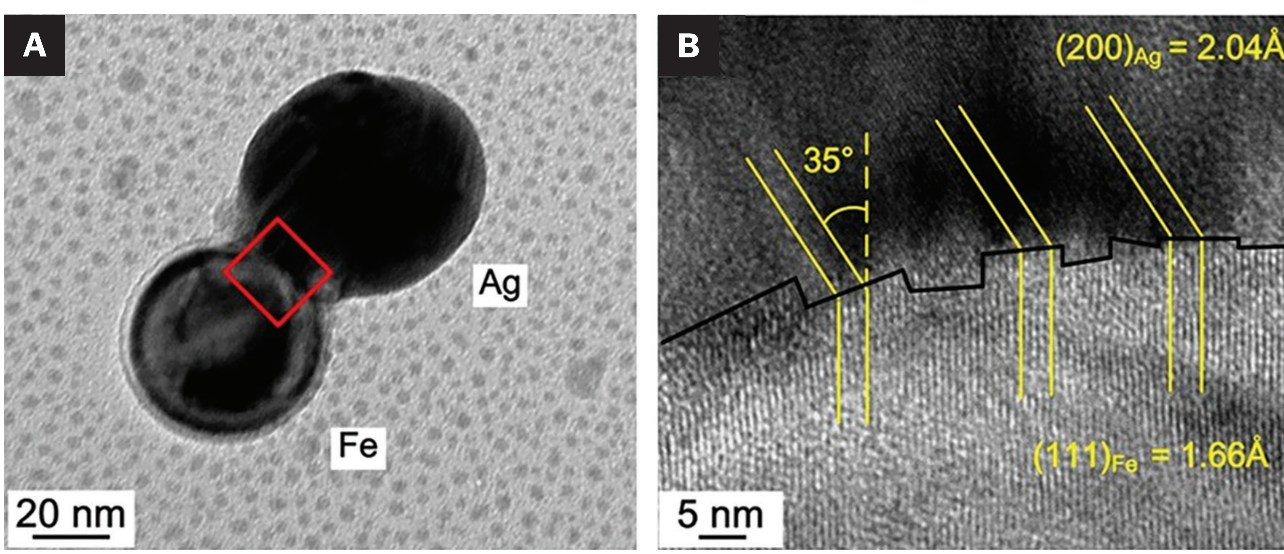

Fig. 18 — A — TEM images of Ag and Fe nanoparticles joined by fs laser radiation; B — high-resolution TEM (HRTEM) image of the Ag-Fe interfacial area within the red square in (A), with yellow lines indicating the plane direction and the black line highlighting structural ledges (Ref. 27).

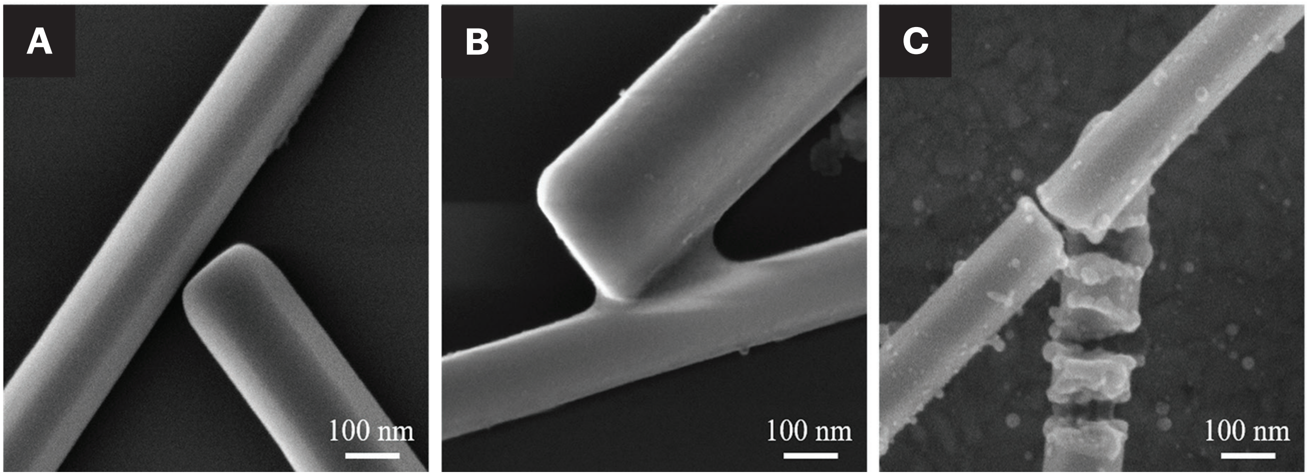

Fig. 19 — Laser joining of ZnO nanowires: A — Before welding; B — successfully welded nanowires; C — over-welding caused by excessive energy density (Ref. 28).

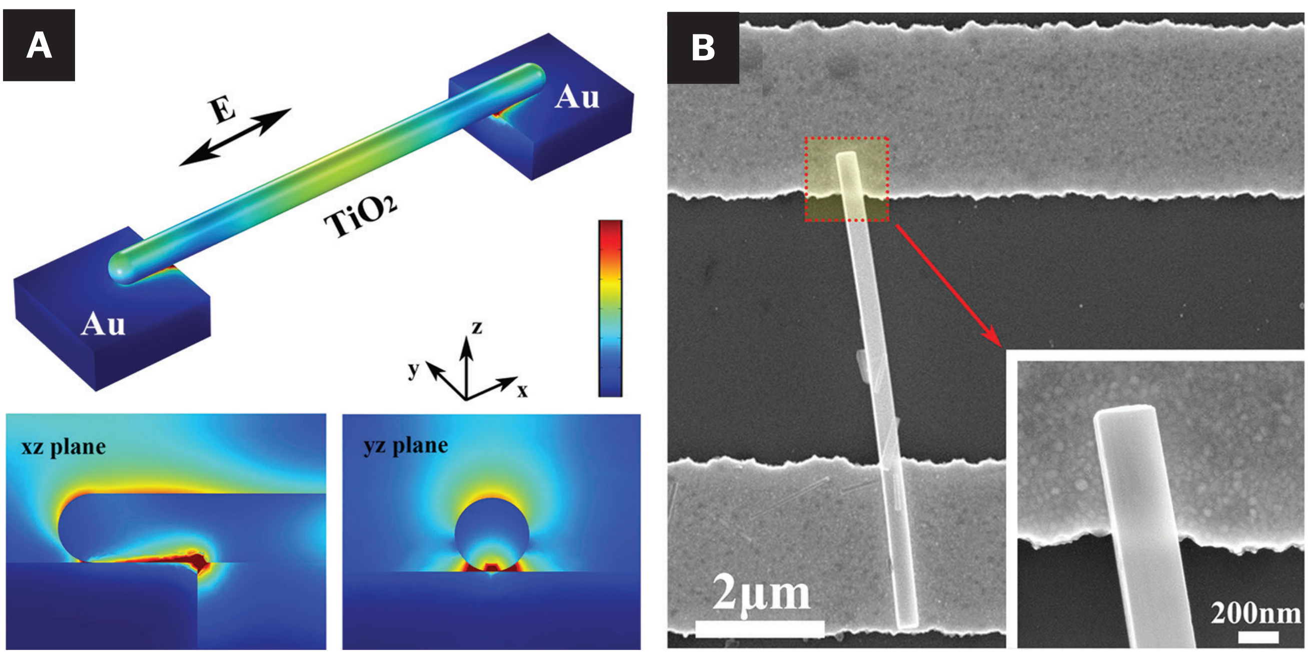

Fig. 20 — A — Simulation of the electric field (|E|) distribution around the laser-irradiated TiO_2 nanowire welded to the Au electrode. The color scale represents the magnitude of the generated electric field, and the double arrow indicates the direction of laser polarization; B — SEM image of a TiO_2 nanowire fs-laser welded to Au substrates with insets showing a magnified view of the joint (Ref. 5).

do plasmonic and excitonic mechanisms play? How do optical forces influence joint formation?

- Ultrafast phenomena: What defines non-thermal processes, and how do they differ fundamentally from thermal melting? How does non-thermal processing affect the mechanical and functional properties of joints?

Although still in its early stages, nanojoining is rapidly advancing with the potential to revolutionize fields such as electronics, photonics, and nanomedicine. Overcoming engineering challenges, refining nanoscale precision, and addressing fundamental scientific questions will be key to its success. As the field progresses, its impact on advanced manufacturing will become increasingly evident where the interface truly defines the device.

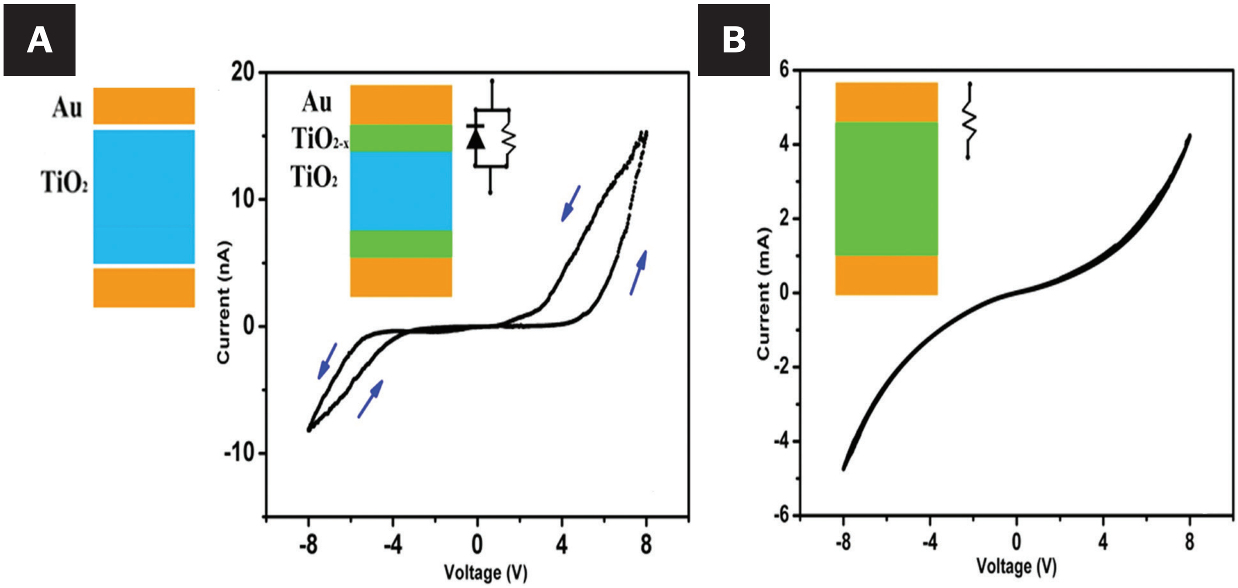

Fig. 21 — Current responses for voltage cycles of 0 V → 8 V → 8 V → 0 V for TiO_2-Au structures after fs laser irradiation at fluences of: A — 18.3; B — 24.7 mJ/cm². Insets show the schematic of laser irradiated structures (TiO_2 sandwiched TiO_{2-x} inner and Au outer layers for A and TiO_{2-x} sandwiched by Au for B, and corresponding electrical conduction models) (Ref. 5).

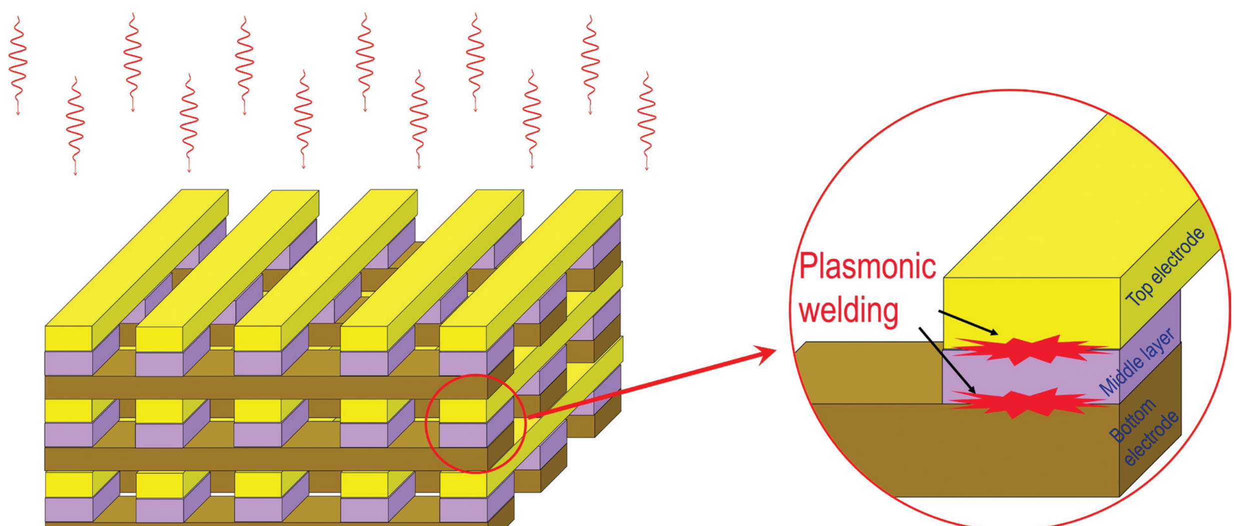

Fig. 22 — Schematic showing connections in a crossbar structure of memristors fabricated using plasmonic welding.

Acknowledgements

The author acknowledges the continuous support from the Natural Sciences and Engineering Research Council of Canada (NSERC) and Canada Research Chairs (CRC) Program. He is also indebted to the support of the AWS Adams Lecture Award and to many years of insightful and mutually stimulating discussions with his students and colleagues.

References

1. American Welding Society. *Welding Handbook* 10(1), 9(2–5). American Welding Society.

2. Liang, B.-S. 2021. Entrepreneurship-driven growth in the integrated circuit design industry. *Nature Electronics* 4: 234–236.

3. Harman, G. 2010. *Wire Bonding in Microelectronics, 3rd Edtion*. McGraw-Hill.

4. Chen, C., Yan, L., Kong, E., and Zhang, Y. 2006. Ultrasonic nano-welding of carbon nanotubes to metal electrodes. *Nanotechnology* 17: 2192–2197.

5. Lin, L., Liu, L., Musselman, K., Zou, G., Duley, W., and Zhou, Y. 2016. Plasmonic-radiation-enhanced metal oxide nanowire heterojunctions for controllable multilevel memory. *Advanced Functional Materials* 26: 5979–5986.

6. Zhou, Y. 2008. *Microjoining and nanojoining*. Woodhead Publishing Ltd./CRC Press.

7. Zhou, Y., and Hu, A. 2011. From Microjoining to Nanojoining. *The Open Surface Science Journal* 3: 32–41.

8. Gösele, U., Stenzel, H., Martini, T., Steinkirchner, J., Conrad, D., and Scheerschmidt, K. 1995. Self-propagating room temperature silicon wafer bonding in ultrahigh vacuum. *Applied Physics Letters* 67: 3614–3616.

9. Terrones, M., Banhart, F., Grobert, N., Charlier, J., Terrones, H., and Ajayan, P. 2002. Molecular junctions by joining single-walled carbon nanotubes. *Physical Review Letters* 89: 075505.

10. Lu, Y., Huang, J., Wang, C., Sun, S., and Lou, J. 2010. Cold welding of ultrathin gold nanowires. *Nature Nanotechnology* 5: 218–224.

11. Liu, L., Shen, D., Zou, G., Peng, P., and Zhou, Y. 2016. Cold welding of Ag nanowires by large plastic deformation. *Scripta Materialia* 114: 112–116.

12. Peng, P., Liu, L., Gerlich, A., Hu, A., and Zhou, Y. 2013. Self-oriented nanojoining of silver nanowires via surface selective activation. *Particle & Particle Systems Characterization* 30(5): 420–426.

13. Yoon, S., and Khang, D. 2016. Room-temperature chemical welding and sintering of metallic nanostructures by capillary condensation. *Nano Letters* 16(6): 3550–3556.

14. Zou, R., Zhang, Z., Xu, K., Jiang, L., Tian, Q., Sun, Y., Chen, Z., and Hu, J. 2012. A method for joining individual graphene sheets. *Carbon* 50(3): 4965–4972.

15. Ide, E., Angata, S., Hirose, A., and Kobayashi, K. 2005. Metal–metal bonding process using Ag metallo-organic nanoparticles. *Acta Materialia* 53(8): 2385–2393.

16. Peng, P., Hu, A., Gerlich, A., and Zhou, Y. 2015. Self-generated local heating induced nanojoining for room temperature pressureless flexible electronic packaging. *Scientific Reports* 5: 9282 (1–7).

17. Gu, Z., Ye, H., Smirnova, D., Small, D., and Gracias, D. 2006. Reflow and electrical characteristics of nanoscale solder. *Small* 2: 225–229.

18. Qu, K., Zhang, H., Lan, Q., Deng, X., Ma, X., Huang, Y., Zhang, J., Ma, H., Inkson, B., Xue, D., and Peng, Y. 2015. Realization of the welding of individual TiO_2 semiconductor nano-objects using a novel 1D $Au_{80}Sn_{20}$ nanosolder. *Journal of Materials Chemistry C* 43(3): 11311–11317.

19. Peng, Y., Cullis, T., and Inkson, B. 2009. Bottom-up nanoconstruction by the welding of individual metallic nanoobjects using nanoscale solder. *Nano Letters* 9(1): 91–96.

20. Mafuné, F., Kohno, J., Takeda, Y., and Kondow, T. 2003. Nanoscale soldering of metal nanoparticles for construction of higher-order structures. *Journal of American Chemical Society* 125(7): 1686–1687.

21. Liu, L., Huang, H., Hu, A., Zou, G., Quintino, L., and Zhou, Y. 2013. Nano brazing of Pt-Ag nanoparticles under femtosecond laser irradiation. *Nano-Micro Letters* 5(2): 88–92.

22. Tohmyoh H., and Fukui, S. 2009. Self completed joule heat welding of ultrathin Pt wires. *Physical Review* B 80: 155403 (1–7).

23. Tohmyoh, H., Imazumi, T., Hayashi, H., and Saka, M. 2007. Welding of Pt nanowires by joule heating. *Scripta Materialia* 57: 953–956.

24. Kim, S., and Jang, D. 2005. Laser-induced nanowelding of gold nanoparticles. *Applied Physics Letters* 86: 033112 (1–3).

25. Garnett, E., Cai, W., Cha, J., Mahmood, F., Connor, S., Christoforo, M., Cui, Y., McGehee, M. D., and Brongersma, M. 2012. Self-limited plasmonic welding of silver nanowire junctions. *Nature Materials* 11: 241.

26. Jiao, Z., Huang, H., Liu, L., Hu, A., Duley, W., He, P., and Zhou, Y. 2014. Nanostructure evolution in joining of Al and Fe nanoparticles with femtosecond laser irradiation. *Journal of Applied Physics* 115: 134305-1–134305-6.

27. Jiao, Z., Sivayoganathan, M., Duley, W., He, P., and Zhou, Y. 2014. Formation and characterization of femtosecond laser induced subcluster segregated nanoalloys. *Journal of Physical Chemistry C* 118: 24746–24751.

28. Xing, S., Lin, L., Zou, G., Liu, L., Duley, W., and Zhou, Y. 2019. Two-photon absorption induced nanowelding for assembling ZnO nanowires with enhanced photoelectrical properties. Applied Physics Letters 115: 103101.

29. Sun, T., Huo, J., Xiao, Y., Liu, L., Feng, B., Zhai, X., Wang, W., and Zou, G. 2022. Atomic bonding-engineered heterogeneous integration of semiconductor nanowires by femtosecond laser irradiation for a miniaturized photodetector. *Applied Surface Science* 575: 151709.

30. Wang, J., Hu, A., Persic, J., Wen, J., and Zhou, Y. 2011. Thermal stability and reaction properties of passivated Al/CuO nano-thermite. *Journal of Physics and Chemistry of Solids* 72: 620–625.

31. Banhart, F. 2001. The formation of a connection between carbon nanotubes in an electron beam. *Nano Letters* 1(6): 329–332.

32. von der Linde, D., Sokolowski-Tinten, D., and Biakowski, K. 1997. Laser-solid interaction in the femtosecond time regime. *Journal of Applied Surface Science* 109/110(1): 1–10.

33. Link, S., Burda, C., Nikoobakht, B., and El-Sayed, M. 2000. Laser-induced shape changes of colloidal gold nanorods using femtosecond and nanosecond laser pulses. *Journal of Physical Chemistry B* 104: 6152–6163.

34. Chevallier, E., Bruyère, V., Bernard, G., and Namy, P. 2019. Femto-second laser texturing prediction using COMSOL Multiphysics. COMSOL. Retrieved February 17, 2025, from *comsol.com/paper/femto-second-laser-texturing-prediction-using-comsol-multiphysics-82611*.

35. Lin, L., Peng, L. L. P., Duley, W., and Zhou, Y. 2016. In situ nano-joining of Y- and T- shaped silver nanowire structures for optical logic applications using femtosecond laser radiation. *Nanotechnology* 27: 125201 (1–11).

36. Johnson, K., and Keller, D. 1967. Effect of contamination on the adhesion of metallic couples in ultra-high vacuum. *Journal of Applied Physics* 38(4): 1896–1904.

37. Xing, S, Lin, L., Zou, G., Liu, L., Duley, W., and Zhou, Y. 2019. Unpublished research.

38. Huang, H., Liu, L., Peng, P., Hu, A., Duley, W., and Zhou, Y. 2012. Controlled joining of Ag nanoparticles with femtosecond laser radiation. *Journal of Applied Physics* 112: 123519-1–123519-4.

39. Chua, L. 1971. Memristor-The missing circuit element. *IEEE Transactions on Circuit Theory* 18(5): 507–519.

40. Strukov, D., Snider, G., Gregory, S., Stewart, D., and Williams, R. 2008. The missing memristor found. *Nature* 453: 80–83.

41. Xia, Q., and Yang, J. 2019. Memristive crossbar arrays for brain-inspired computing. *Nature Materials* 18: 309–323.

Y. NORMAN ZHOU (*nzhou@uwaterloo.ca*) **is with the University of Waterloo, Waterloo, Ontario, Canada.**